



An experimental study on the drilling of CFRP sandwich structures with filled and unfilled aramid honeycomb cores

Norbert Geier¹

Received: 8 October 2022 / Accepted: 6 March 2023
© The Author(s) 2023

Abstract

Lightweight carbon fibre-reinforced polymer (CFRP) sandwich structures with honeycomb cores have excellent specific bending stiffness and good dimensional stability; therefore, their future applications will extend extensively, despite their difficult-to-manufacture nature. Although the drilling of single CFRP structures has been widely investigated, the published experience of drilling honeycomb cored CFRP sandwich panels is strongly limited. Therefore, the main objective of the present paper is to experimentally analyse the machinability of CFRP sandwich panels with filled and unfilled aramid Cormaster honeycomb cores through the analysis of thrust force, drilling torque and drilling-induced burrs. A twist and a brad and spur drill were used in two sandwich structures at three feed levels for the drilling experiments. The thrust force and drilling torque were measured by a KISTLER dynamometer, and the burrs were processed through digital image processing of optically captured images. The experimental results show that the application of fillers in the honeycomb only slightly decreases the nominal specific stiffness of the CFRP/honeycomb sandwich structures and slightly increases the thrust force; however, a significant improvement is achievable by their application in the drilling-induced burr formation of the honeycomb core.

Keywords CFRP · Sandwich structure · Honeycomb core · Cutting force · Burrs

1 Introduction

Lightweight polymer composite sandwich structures have excellent flexural rigidity to weight ratio, outstanding corrosion resistance, unique resilience and shock absorption, and good dimensional and chemical stability [1–3]. Therefore, these sandwich structures are widely used in high-end industries such as aerospace, automobile and shipbuilding [4, 5]. The polymeric sandwich structures are often built up by high strength carbon fibre-reinforced polymer (CFRP) composite skins and low-density aramid honeycomb core materials [6]. These CFRP/honeycomb sandwich structures have to be often mechanically machined to meet dimensional and functional requirements [7, 8]. However, the machining of

CFRP/honeycomb structures is challenging mainly because (i) the aramid honeycomb structure is non-homogeneous, anisotropic and thin-walled [6, 9, 10], (ii) the CFRP shells are non-homogeneous, anisotropic and highly abrasive [11–14], and (iii) the machining-induced chips pollute the environment and hurt human health [15]. Despite the latter challenge is often solved easily by the application of an industrial vacuum cleaner, the i) and ii) challenges cannot be solved by any easy-to-implement technology, as their aspects and requirements often contract each other's (e.g. the honeycomb requires thin and sharp straight blade cutting tool [16]; however, the CFRP requires a more robust cutting geometry due to larger cutting forces and significant tool wear [17]).

Xu et al. [9] conducted machining experiments in a Nomex honeycomb core and analysed the influences of the cutting angles, entrance angle and engagement angle on the cell wall deformation, cutter-workpiece interaction and the thin-walled cell geometry. Using an optimised up-milling process, they could reduce the damage size by at least 40%. They highlighted that the cutting directions and the tool geometry have a significant influence on the chip formation mechanisms. Xiang et al. [18] highlighted that high-speed milling of aramid honeycomb structures is time-consuming,

Technical Editor: Adriano Fagali de Souza.

✉ Norbert Geier
geier.norbert@gpk.bme.hu

¹ Department of Manufacturing Science and Engineering, Faculty of Mechanical Engineering, Budapest University of Technology and Economics, Műegyetem rkp. 3., Budapest 1111, Hungary

resulting in serious machining-induced defects and environmental pollution problems. Therefore, ultrasonic vibration-assisted (UVA) machining is the suggested technology to cut aramid honeycomb structures. Xiang et al. analysed and optimised ultrasonic longitudinal-torsional vibration-assisted machining technology using a special disc cutting tool to effectively cut the thin-walled aramid honeycomb. They found that the cutting force was more influenced by the cutting speed than the feed. UVA straight blade cutting tools are also efficient for cutting aramid honeycomb structures [6]. Although the UVA machining is an effectively applicable technology in the cutting of single honeycomb structures and the drilling of single CFRPs too [19, 20], the directions—relative to the axis of the honeycomb pockets—of cutting feed and vibration differ: the honeycomb is often cut in a perpendicular direction [6], but the CFRPs have to be machined from a parallel direction [11]. This makes the design of the machining process of combined CFRP/honeycomb structures even more difficult.

Hole machining in CFRPs is often performed by conventional drilling operations. Therefore, this technology seems to be promising in the hole-making in CFRP/honeycomb sandwich structures. Nevertheless, as the aramid honeycomb structure does not support the radial crushing force [21, 22], and the radial forces of mechanical drilling are considerable, a huge machining-induced deformation of the honeycomb structure is expected. Although the hole machining in CFRP/honeycomb structures is of great interest to industry and academy, the number of published studies on the drilling polymeric honeycomb sandwich structures is few.

Lindqvist et al. [23] reported a technical paper on the conventional drilling versus helical milling (also known as orbital drilling) of CFRP/honeycomb sandwich panels and analysed the effect of the technologies on the delamination, hole diameter, ovality of the holes and tool wear. They could achieve delamination-free sharp and clear holes by the helical milling technology. Kihlman et al. [24] conducted helical milling experiments in CFRP/honeycomb sandwich panels using industrial robots and measured the cutting forces. They observed almost eight times smaller forces through helical milling than conventional drilling. However, they highlighted that the robotic deflection is a recent issue has to be improved in order to implement helical milling in industry. Lindqvist and Kihlman [25] provided later a study on the implementation and evaluation of helical milling in CFRP/honeycomb structures. They could improve the control (i.e. positioning of the tool) of helical milling using expensive drill jigs. Yang et al. [26] conducted machining experiments in CFRP/honeycomb sandwich structures and analysed the influences of the technological parameters, support conditions and honeycomb core thickness on the thrust force and delamination area. They proved that the feed significantly influenced the thrust force and observed that the

damage magnitude of the honeycomb core decreases with core thickness. Zarrouk et al. [10] optimised the milling of Nomex honeycomb structures by analysing cutting force and chips morphology. Their results are in good agreement with Yang's results: the larger the feed and the lower the cutting speed, the larger the cutting force is. Khoran et al. [27] conducted drilling experiments in sandwich structures having glass fibre-reinforced polymer (GFRP) composite shells but different core materials: (i) polyvinyl chloride (PVC) foam, (ii) balsa wood and (iii) corrugated-foam core made of glass/polyester (trapezoidal corrugated section) and PVC foam. They analysed the effect of process parameters on machining-induced burr and delamination characteristics. They found that the feed has the most significant influence on delamination and burr. Furthermore, they could drill the best quality holes in the balsa wood composite panels.

Most of the relevant scientific literature reports on the mechanical properties of CFRP/honeycomb sandwich structures or the machining challenges and modelling of polymeric/honeycomb sandwich structures. However, it is difficult to find any experience in drilling CFRP/honeycomb sandwich structures considering different honeycomb cores. The more profound understanding of the drilling process of CFRP/honeycomb sandwich structures indicates the relevancy of the present study: the main aim is to analyse the influences of drilling tool geometries and feed on the thrust force, drilling torque and machining-induced burrs in CFRP sandwich structures with filled and unfilled aramid honeycomb cores. In an attempt to achieve this aim, mechanical drilling experiments were carried out using two different drilling tools in filled and unfilled CFRP/honeycomb sandwich structures and analysed through digital images processing (DIP) and analysis of variance (ANOVA).

2 Experimental setups

2.1 Workpieces

The machining experiments were conducted in two different carbon fibre-reinforced polymer (CFRP) sandwich structures with honeycomb cores. The sandwich structures were built using unidirectional (UD) and multidirectional (MD) prepreg CFRP sheets and Cormaster N636-CN1 honeycomb structure made from para-aramid N636 DuPont paper sheets and phenolic resin. The nominal wall thickness (t), cell size and the density of the honeycomb core were 0.35 mm, 3.2 mm and 64 kg/m³, respectively. One of the cores of the sandwich structures was filled with the mix of epoxy resin (EC 130 resin and W340 hardener with a ratio of 100:33) and micro-glass balloons (Q-CELL) in order to improve the stiffness of the sandwich structure. The filler could be penetrated only from the laminating direction; thus,

the core could not be totally filled mainly due to the quasi-high viscosity of the filler (Fig. 1b). The cross sections of the applied composite structures are shown in Fig. 1, and the layer sequence is listed in Table 1. The prebuilt sandwich structures were cured in an Olmar ATC 1100/2000

autoclave for $t=5$ h at $T=160$ °C in $p=2$ bar. The cured sandwich structures were cut using a diamond disc saw into $25 \times 50 \times 200$ mm pieces to meet the dimensional requirements of the applied machining fixture (see in Fig. 2a).

Fig. 1 Representative cross sections of the applied **a** A: CFRP/honeycomb and **b** B: CFRP/filled honeycomb sandwich structures; and **c** C single aramid honeycomb structure

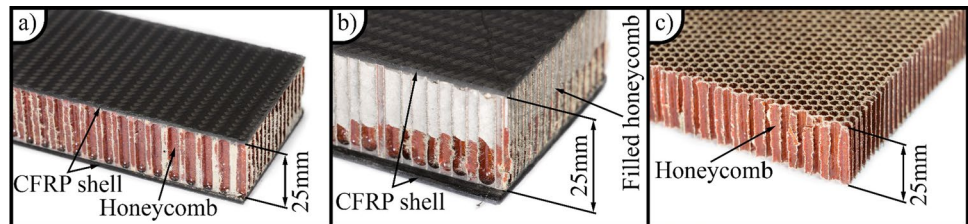


Table 1 Layer sequence of the applied CFRP sandwich structures

No	A: CFRP/honeycomb sandwich		B: CFRP/filled honeycomb sandwich	
	Name	Type	Name	Type
1	SC-160 245g twill	MD prepreg	SC-160 245g twill	MD prepreg
2	SC-160 300g UD	UD prepreg	SC-160 300g UD	UD prepreg
3	SC-160 300g UD	UD prepreg	SC-160 300g UD	UD prepreg
4	SC-160 300g UD	UD prepreg	SC-160 300g UD	UD prepreg
5	SC-160 245g twill	MD prepreg	SC-160 245g twill	MD prepreg
6	SA 80	Honeycomb glue	SA 80	Honeycomb glue
7	N636 CN1 3.2–64, 21.6 mm	Honeycomb core	N636 CN1 3.2–64, 21.6 mm + Epoxy resin + Q-CELL	Honeycomb core with filler
8	SA 80	Honeycomb glue	SA 80	Honeycomb glue
9	SC-160 245g twill	MD prepreg	SC-160 245g twill	MD prepreg
10	SC-160 300g UD	UD prepreg	SC-160 300g UD	UD prepreg
11	SC-160 300g UD	UD prepreg	SC-160 300g UD	UD prepreg
12	SC-160 300g UD	UD prepreg	SC-160 300g UD	UD prepreg
13	SC-160 245g twill	MD prepreg	SC-160 245g twill	MD prepreg

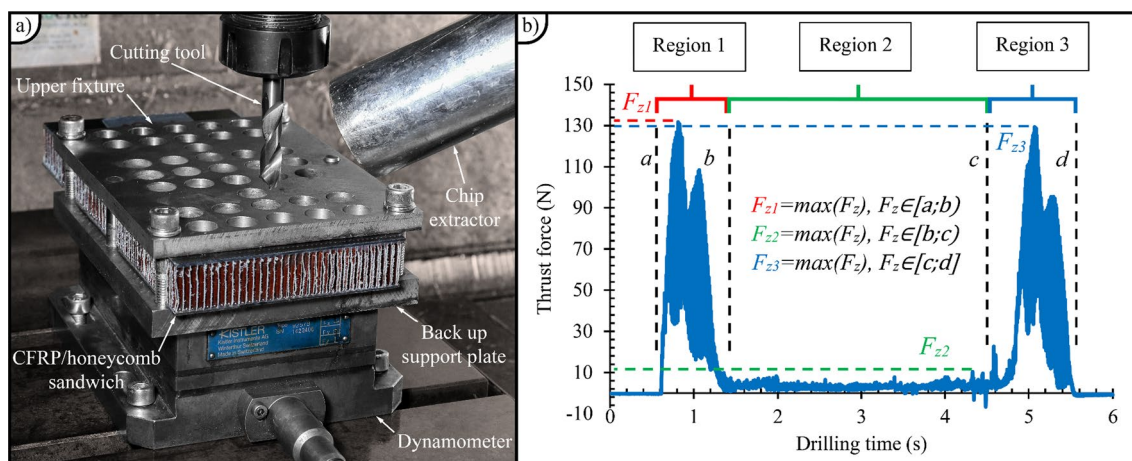


Fig. 2 **a** The experimental machining setup; **b** the interpretation of the thrust forces in each three regions

Bending stiffness (K) of the applied structures was determined by three-point flexural tests according to the ISO 178:1996 standard using a Zwick Z050 tester. The tests were repeated five times in each sandwich structure, and the average was calculated. The tests resulted in $K_A = 116.5 \pm 3.9$ MPa and $K_B = 142.0 \pm 6.7$ MPa bending stiffnesses for the non-filled and the filled CFRP sandwich structures, respectively. The specific bending stiffness (k) is calculated as expressed by Eq. (1).

$$k = \frac{1}{5} \frac{\sum_{i=1}^5 K_i}{\sum_{i=1}^5 m_i} \quad (1)$$

where m denotes the mass of the sandwich workpieces, and $n=5$ is the number of repeated three-point flexural tests. The specific stiffness results are $k_A = 1.51 \pm 0.02$ MPa/kg and $k_B = 1.19 \pm 0.05$ MPa/kg. The mass of each workpiece was measured by an Ultra Ship-55 digital scale.

2.2 Machines, tools and equipment

The nominal diameter of $d_{\text{hole}} = \varnothing 10$ mm holes was drilled on a three-axis Kondia B640 CNC machining centre with a maximum spindle speed of $n = 12,000$ rpm and spindle power of $P = 15$ kW. The workpiece was fixed in a special fixture designed to provide balanced support of the top and bottom layers of the CFRP shells against buckling at



Fig. 3 Illustration of the applied drilling tools: **a** T1: twist drill, **b** T2: brad and spur drill

the entry and exit of the holes, respectively. The fixture was installed onto a KISTLER 9257BA three-component dynamometer. The drilling-induced chips were removed by a Nilfisk GB733 industrial vacuum cleaner. The experimental machining setup is shown in Fig. 2a.

Two types of drilling tools were applied for the experiments: a conventional twist drill (denoted by T1) and a brad and spur drill (denoted by T2). The applied cutting tools are illustrated in Fig. 3, and their main properties are listed in Table 2. Both cutting tools are uncoated solid carbide drills with a nominal diameter of $d_{\text{tool}} = \varnothing 10$ mm. The brad and spur drill was selected because it has a favourable “cut first, push second” phenomena [28], that is expected to result in less drilling-induced burrs and delamination in FRPs [17]. The conventional twist drill geometry was selected to have a reference, as working experiences with twist drills are relatively deep [29]. Mainly due to the excellent wear resistance of the selected tools and the relatively low number of experimental runs, the tool wear was unexpected; however, the tool condition was monitored after each drilling operation. The main cutting edges of the tools were photographed using a Dino-Lite AD7013MZT digital microscope, and the evolution of the contour of the main cutting edge is analysed through digital image processing (DIP). The results show that the tool wear is negligible; therefore, the experimental results do not have to be compensated.

The thrust force (F_z) was measured by a KISTLER 9257BA dynamometer, processed through a KISTLER 5070 multi-channel charge amplifier, a National Instruments USB-4431 dynamic signal acquisition module and LabVIEW software. The sampling frequency was set to $f_s = 4\,000$ Hz. The collected data were cut and filtered by fast Fourier transformation-based (FFT) Butterworth low pass filter at the cut-off frequency of $f_c = 200$ Hz. The interpretation of thrust force is illustrated in Fig. 2b. As a consequence of the inhomogeneous but symmetrical structure of the workpieces, three regions were defined, and the responses were calculated in each region. F_{z1} denotes the maximal thrust force in the first

Table 2 The main properties of the applied drilling tools

Property	Tool 1	Tool 2
Type	Conventional twist drill	Brad and spur drill
Shape of the drill tip	Conventional V	Advanced W
Manufacturer and catalogue code	TIVOLY 82439211000	THOMAS TDM PWK 23C103100
Diameter (mm)	$\varnothing 10$	$\varnothing 10$
Material	Uncoated solid carbide	Uncoated solid carbide
Point angle ($^\circ$)	118	Vary
Helix angle ($^\circ$)	25	30

region, F_{z2} is the maximal thrust force in the second region, and so on.

The drilling torque (M) was calculated through the signals of the piezoelectric sensors of the dynamometer and considering the location of the holes, according to the Kistler

Manual Guide and basic mechanics. The drilling torques were calculated by Eq. (2) and Eq. (3).

$$M = \sum_{i=1}^4 k_i \cdot F_i \tag{2}$$

$$M = a \cdot (F_{y1} + F_{y4}) + b \cdot (F_{x3} + F_{x4}) - c \cdot (F_{y2} + F_{y3}) - d \cdot (F_{x1} + F_{x2}) \tag{3}$$

where k denotes the length of the distance vector (the distance from the sensor to the point where force is applied), F is the belonging force component, and $\{a, b, c = 60 - a, d = 115 - b\}$ parameters define the drilling position, as illustrated in Fig. 4.

The drilling-induced burr was examined by the analysis of the burr factor (F_b) and the contour burr factor (F_{bc}), as expressed by Eqs. (2) and (3), respectively.

$$F_b = \frac{A_b}{A_{nom}} \cdot 100 \tag{4}$$

$$F_{bc} = \frac{C_b - C_{nom}}{C_{nom}} \cdot 100 \tag{5}$$

where A_b denotes the burr area, and $A_{nom} = d_{hole}^2 \pi / 4 \approx 78.53 \text{ mm}^2$ is the nominal area of the hole, C_b is the length of the drilled hole-contour, and $C_{nom} = d_{hole} \pi \approx 31.42 \text{ mm}$ is the nominal length of a nominal hole-contour, as illustrated in Fig. 5.

The burr area and the length of the drilled hole-contour were measured and calculated through digital image

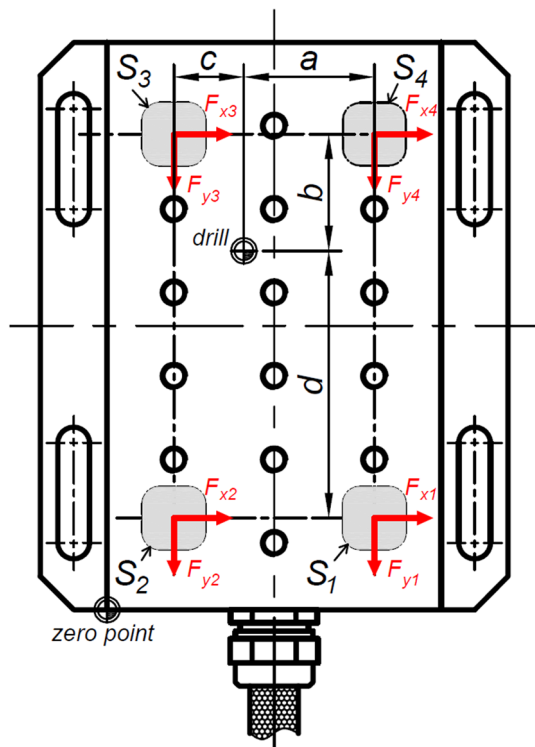


Fig. 4 Illustration of the geometrical parameters used for drilling torque calculations, where S_i denote the piezoelectric sensors

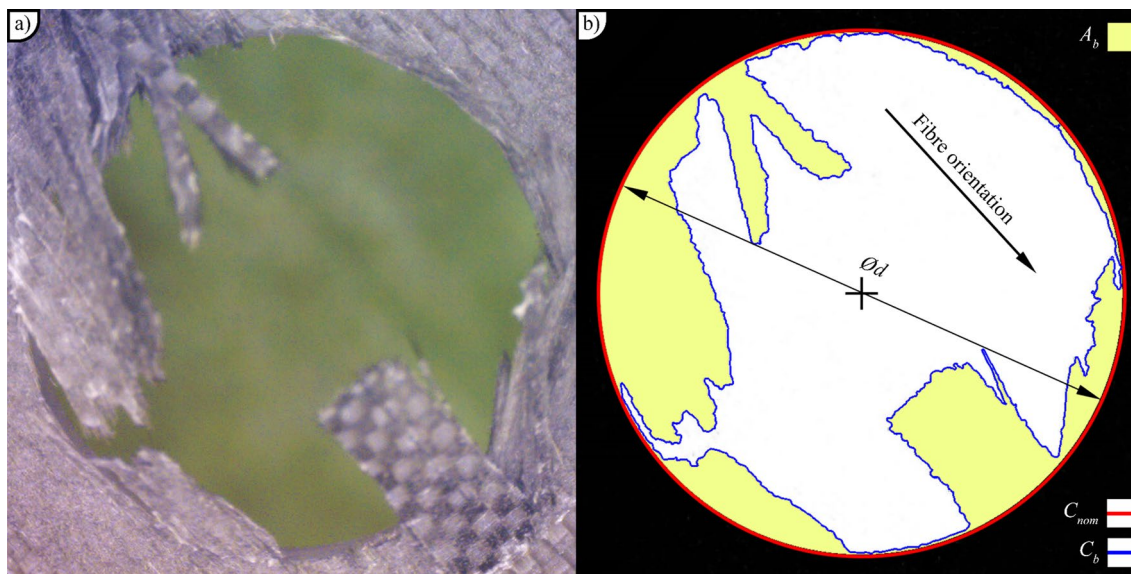


Fig. 5 A schematic illustration of the geometrical parameters used for calculations of burr measures, redrawn based on Ref. [11]

processing of optically captured images (magnification of 30×) of the entry of the holes, using a Dino-Lite AD7013MZT digital microscope. The applied DIP process is described in previous publications of the author [30, 31].

2.3 Conditions and design of experiments

An industrial vacuum cleaner was applied to remove carbon dust from the cutting space; therefore, the drilling experiments were carried out in a dry condition. Considering that the cutting tool geometry and the feed has the most significant influence on the drilling ability of different sandwich structures [26, 32], these factors were selected to examine in this study. The levels of technological parameters were selected based on recommendations of tool manufacturers and previous studies. The cutting speed was fixed to $v_c = 100$ m/min ($n = 3183$ rpm ≈ 53 Hz). The feed (f) was varied at three levels based on the full factorial design. The factors and their levels are shown in Table 3. In order to analyse and somehow prevent (compensate) the influence of the top CFRP shell on the response variables in the second region (F_{z2} and M_2), control experiments were conducted in a single honeycomb structure (denoted by C, illustrated in Fig. 1c). Each experiment at the middle feed level ($f = 0.1$ mm/rev)

was repeated five times to ensure the required repetitions for the analysis of variances (ANOVA) technique. A significance level of $\alpha = 0.05$ was applied in each statistical analysis. The experiments were run in random order to reduce systematic errors.

3 Results and discussion

3.1 Analysis of thrust force and drilling torque

The cutting force and torque of the machining processes are the indicators of the machinability of materials, which are closely correlated to the cutting energetics and chip removal mechanisms [33–35]. Figure 6 shows the influence of the feed (f) and the workpiece ($W = \{A, B, C\}$) on the thrust force (F_z) in different regions of the drilling process. The experimental results show that the larger the feed, the larger the thrust force is in the case of (i) the first and third regions of sandwich A and (ii) each region of sandwich B. This is in a good correlation to the cutting theory, as the larger the feed, the larger the chip cross section and, therefore, the larger the energy demand to remove it [30]. In addition to the expected effect of feed on the thrust force, it was proved statistically that the influence of feed on the thrust force is significant in the CFRP shells, but it is not significant in the honeycomb core (second region in sandwich A and material C), according to the ANOVA results (Table 4a).

Despite that, the main effect plot in Fig. 7 indicates that the effect of feed on the F_z is monotone in each sandwich structure; the reproducibility resulted in relatively large deviations that make this effect insignificant in region 2 (P value = 0.147). The reason for this may be that the honeycomb structure resulted in a difficult-to-controlled

Table 3 Level of factors

Factors			Levels		
			1	2	3
Feed	f	(mm/rev)	0.04	0.1	0.16
Cutting tool	T	(–)	T1	T2	
Workpiece	W	(–)	A	B	C

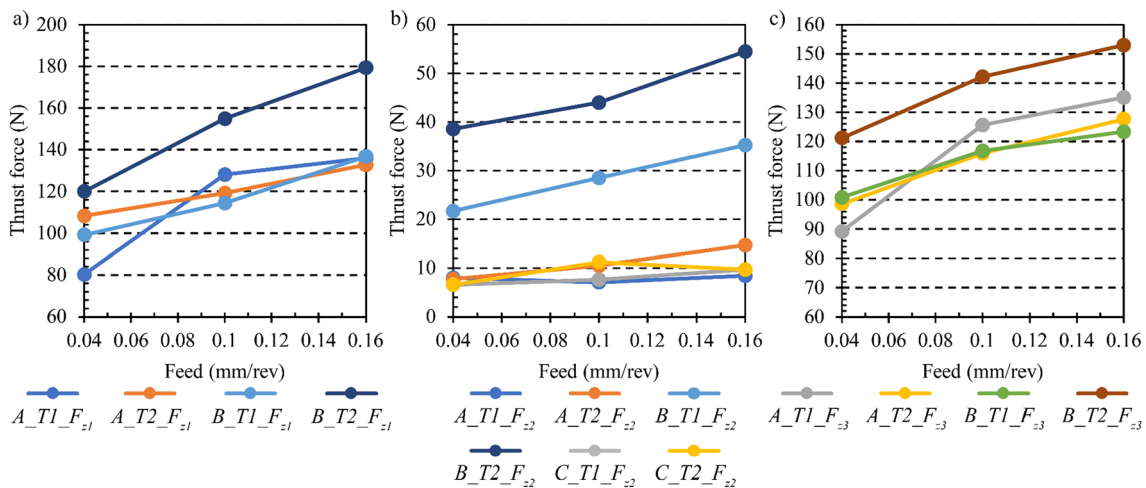


Fig. 6 The influence of the feed and workpiece on the thrust force in the **a** first and third regions and **b** in the second region

Table 4 ANOVA tables for thrust force and drilling torque vs feed, tool and workpiece

(a) Thrust force (F_z)						(b) Drilling torque (M)					
Source	DF	Adj SS	Adj MS	F value	P Value	Source	DF	Adj SS	Adj MS	F value	P value
F_{z1} vs $f = \{f_1, f_2, f_3\}, T = \{T1, T2\}$ and $W = \{A, B\}$						M_1 vs $f = \{f_1, f_2, f_3\}, T = \{T1, T2\}$ and $W = \{A, B\}$					
f	2	4064	2031.8	8.31	0.002	f	2	0.1853	0.0926	81.64	0.000
T	1	2161	2161.3	8.84	0.007	T	1	0.1522	0.1522	134.18	0.000
W	1	1264	1264.2	5.17	0.033	W	1	0.0016	0.0016	1.45	0.240
Source	DF	Adj SS	Adj MS	F value	P value	Source	DF	Adj SS	Adj MS	F value	P value
F_{z2} vs $f = \{f_1, f_2, f_3\}, T = \{T1, T2\}$ and $W = \{A, B, C\}$						M_2 vs $f = \{f_1, f_2, f_3\}, T = \{T1, T2\}$ and $W = \{A, B, C\}$					
f	2	154	77	2.03	0.147	f	2	0.0063	0.0031	6.28	0.005
T	1	571.2	571.17	15.04	0.000	T	1	0.0014	0.0014	2.95	0.095
W	2	7063	3531.51	92.97	0.000	W	2	0.2707	0.1353	269.57	0.000
Source	DF	Adj SS	Adj MS	F value	P value	Source	DF	Adj SS	Adj MS	F value	P value
F_{z3} vs $f = \{f_1, f_2, f_3\}, T = \{T1, T2\}$ and $W = \{A, B\}$						M_3 vs $f = \{f_1, f_2, f_3\}, T = \{T1, T2\}$ and $W = \{A, B\}$					
f	2	2327	1163.48	9.32	0.001	f	2	0.2598	0.1299	47.57	0.000
T	1	605	604.98	4.85	0.038	T	1	0.3000	0.3000	109.88	0.000
W	1	647.1	647.07	5.18	0.032	W	1	0.0266	0.0266	9.75	0.005

honeycomb cutting angle (θ —the angle between the cutting speed and the honeycomb wall). This phenomenon is discussed in Sect. 3.3.

The difficult-to-perform nature of controllability and predictability of thrust force of the hollow core honeycomb structure can be improved by applying fillers in the core. Although the specific stiffness of the B (filled) sandwich panel is smaller ($k_B < k_A$), the cutting mechanism is expected to be better due to the more homogeneous structure. Therefore, the influence of feed on the thrust force was found significant in the case of the B sandwich structure, as shown in Fig. 6b.

The influence of the tool on the thrust force is significant according to the main effect plots and ANOVA tables in Fig. 7 and Table 4a, respectively. The thrust forces of T1 were found smaller than that of T2. Both cutting tools are uncoated solid carbide tools with sharp cutting edges, thus a favourable choice for composite machining. However, the brad and spur drill (T2) is advantageous mainly from the point of view burr and delamination minimisation [36] and not from the thrust force minimisation. The smaller the point angle of a twist drill, the smaller the thrust force is in the drilling of CFRPs, according to Gaitonde et al. [37]. As the point angle of tool T1 is relatively small, the thrust force is small. In summary, the T1 tool is suggested to apply to minimise thrust force at a fixed material removal rate.

The experimental results show that the influence of the workpiece on the thrust force is significant according to the main effect plots and ANOVA tables in Fig. 7 and Table 4a, respectively. The thrust force in sandwich B was more prominent than in sandwich A, because the more the filler, the

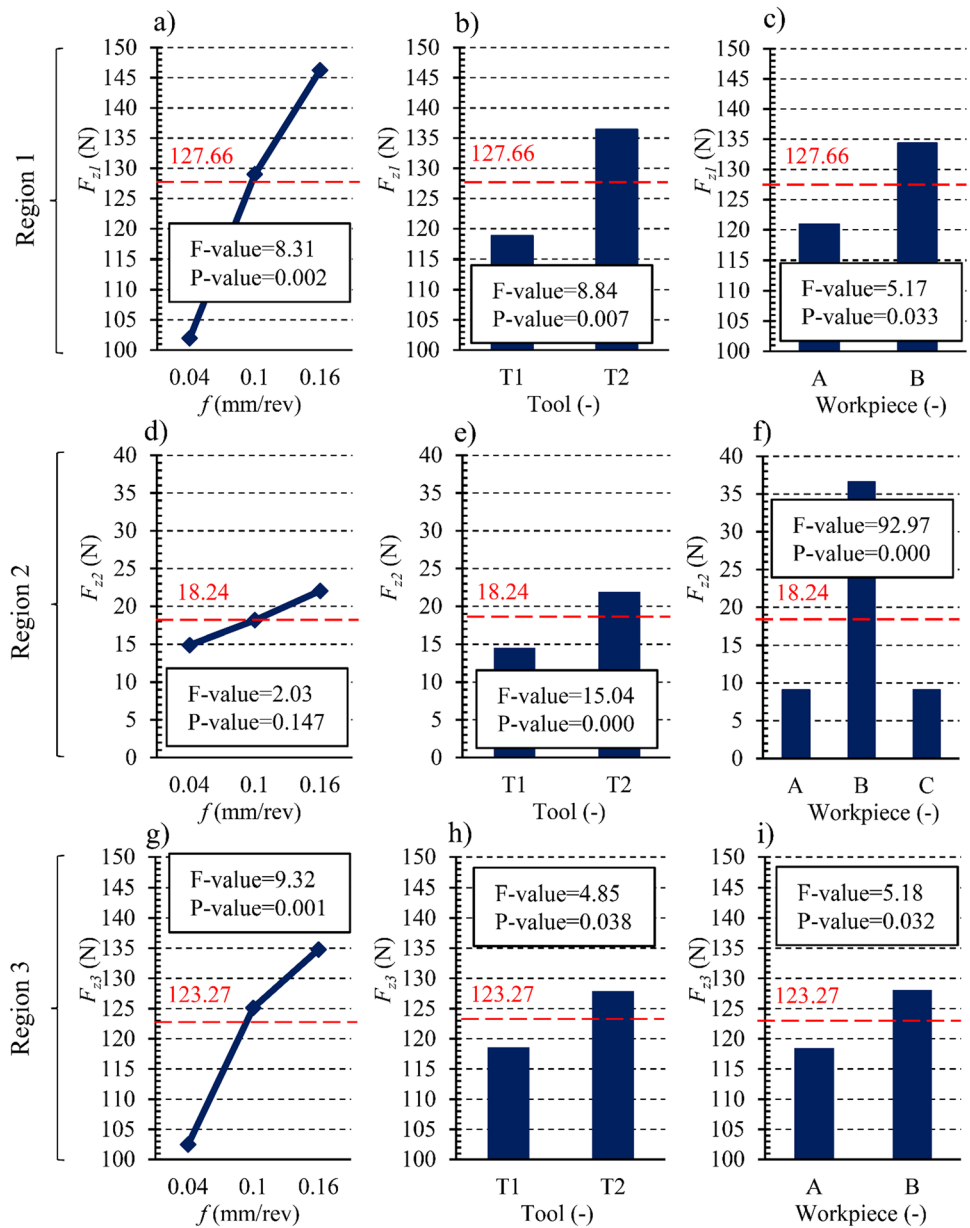
less the air in the core and thus the larger the energy demand of chip removal is.

The drilling torque results, main effect plots and ANOVA tables are shown in Figs. 8, 9 and Table 4b, respectively. According to the results of ANOVA, the cutting tool has the most significant influence on the drilling torque in the CFRP shells, followed by the feed and the workpiece, respectively. As it can be seen in the drilling torque diagrams in Fig. 8, the larger the feed, the larger the torque is, as it is expected based on the thrust force results.

As the nominal thicknesses of the CFRP shells of sandwich A and B are identical, the drilling torque is similar in the first and last regions. Nevertheless, the influence of the workpiece on the drilling torque is significant in the core (second) region, according to the main effect plots and ANOVA tables in Fig. 9 and Table 4b, respectively. The filled sandwich structure required more drilling torque than the unfilled one, as expected due to the larger chip cross section, as explained in the thrust force results.

The significant cross-effects of the factors on the thrust force and drilling torque are shown in Fig. 10. The ANOVA resulted in that (i) the cross-effects of W - T on the thrust force are significant in each region, (ii) the cross-effect of f - T on the drilling torque is significant in the first region and (iii) the W - T 's in the second region. The cross-effect analysis indicates that the effect of the workpiece on the F_z and M parameters significantly depends on whether the T1 or T2 is applied. Furthermore, the T1 is the best choice from the point of view of minimal thrust force and torque; nevertheless, each cutting tool seems to be advantageous in sandwich

Fig. 7 The main effect plots for the thrust force (F_z) in each region



A. Therefore, the burr formation ability of the different technologies is analysed in the next section to deeper understand the workability of the cutting tools and the machinability of the sandwich structures.

3.2 Analysis of drilling-induced burrs

Representative processed images of drilled holes in the analysed structures are summarised in Fig. 11. The burr factor (F_b) and contour burr factor (F_{bc}) were calculated for the sandwich A and B structures according to Eqs. (4) and (5). According to the main effect plots (Fig. 12) and ANOVA tables (Table 5), the tool has the most significant influence on the burr factor, followed by the workpiece,

but the feed does not significantly influence the burr factor. Despite the larger the feed, the larger the thrust force and torque, the burr formation of composites depends mainly on the tool geometry, the directions of cutting and the mechanical supporting properties of the uncut material [11, 38]. The main effect of the factors on the contour burr factor is similar to the burr factor, but the workpiece has a more significant effect than the tool. Although the burr characteristics were not calculated in the single honeycomb structure (C) due to structural difficulties, the processed images in Fig. 11 suggest that T2 could cut the honeycomb structure more effectively than T1.

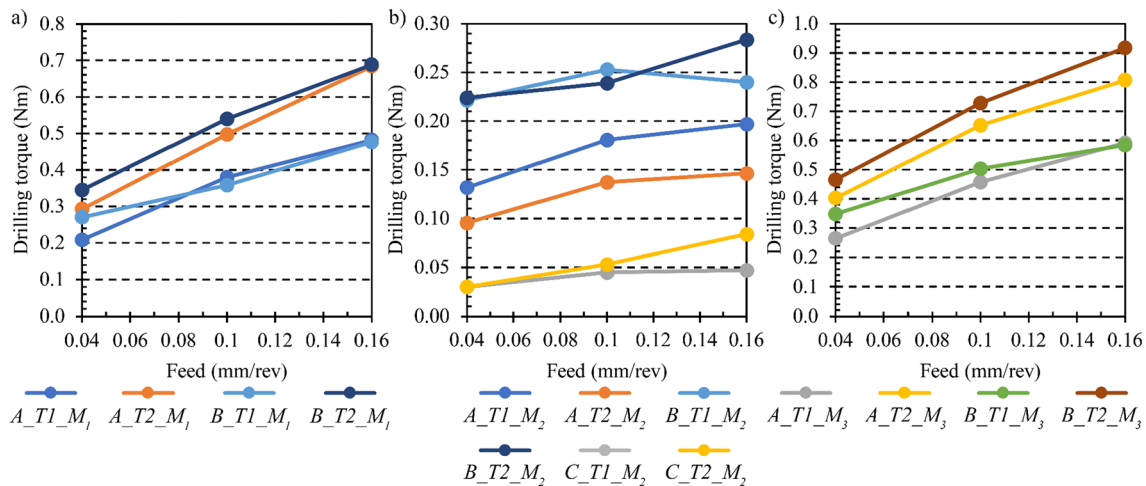


Fig. 8 The influence of the feed and workpiece on the drilling torque in the **a** first and third regions and **b** in the second region

The main effect plots in Fig. 12 show that the F_b and F_{bc} parameters are larger in the unfilled sandwich structure (A) than in the filled one (B). This difference lies in the better mechanical supporting circumstances of the honeycomb walls in the filled structure. The fillers supported the honeycomb structure against buckling; therefore, the cutting edge could cut the honeycomb closer to the nominal depth and result in fewer burrs, as illustrated in Fig. 13.

The T1 produced more drilling-induced burrs than T2, as shown in Fig. 12 a, c. The possible reason for this phenomenon may be found in the cut-first push-second effect of the brad and spur drill geometry, as explained by Su et al. [28]. Therefore, the T2 geometry is more advantageous from the point of view burr formation in each analysed sandwich structure.

The scatterplot of F_b and F_{bc} is shown in Fig. 12e. This diagram shows the achievable quality of drilled holes in sandwiches A and B. The correlation of F_b and F_{bc} is quasi-linear in the case of sandwich B and T2, which means that a larger burr factor (which is proportional to the amount of burrs) results in a larger contour burr factor (which is proportional to the level of burrs destruction [11]) and vice versa. Nevertheless, the F_b and F_{bc} factors do not correlate with each other in the other cases, as Fig. 12e illustrates. It means that the expected burr factor cannot be estimated through knowing the contour burr factor and vice versa. Therefore, both F_b and F_{bc} factors are recommended to be determined for process analysis and quality optimisation in CFRP sandwich structures with honeycomb cores.

3.3 Discussion and outlook

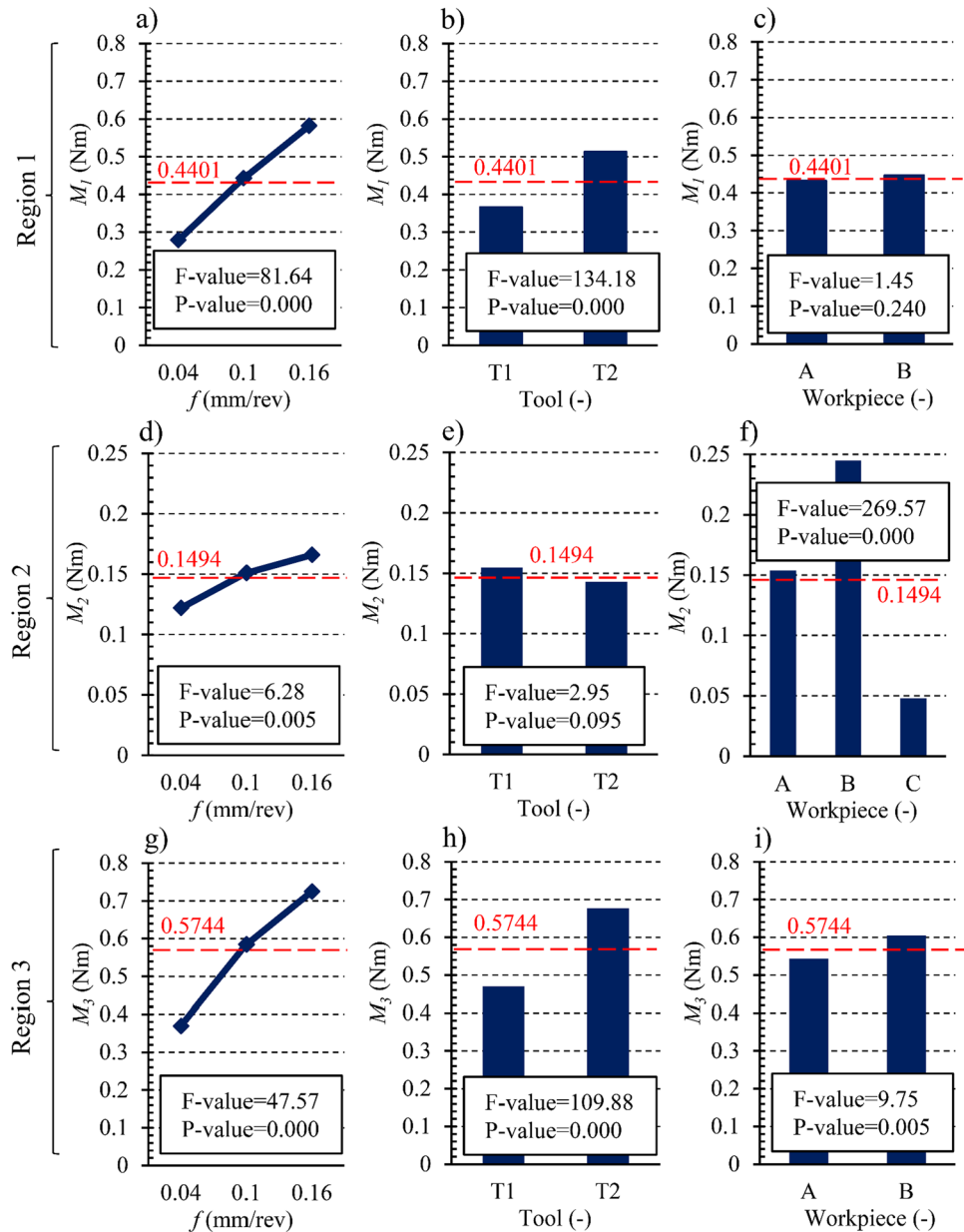
The structural complexity of the CFRP/honeycomb sandwich structures resulted in difficult machinability. It was found that the twist drill (T1) is more advantageous in the

drilling of the CFRP shells, as the achievable hole quality is excellent, and the thrust force and drilling torque are minimal. Nevertheless, the brad and spur drill (T2) produced lower machining-induced burrs in the core of the sandwich structure. These observations result in contradictory requirements of tool selection for unfilled CFRP/honeycomb structures. Although the application of fillers decreases the specific stiffness of the sandwich structures slightly, it can significantly decrease the probability of burr formation in the core material. Therefore, the tool selection of filled CFRP/honeycomb sandwich structures is not as contradictory: applying a twist drill may be the best selection. Although the burr results in Fig. 11 show that the burr area in the B workpiece—using T1—is considerable, it could be significantly decreased by the proper filling of the honeycomb core. This is one of the main future research directions to improve the impregnation of fillers into the honeycomb cores by the proper set and control of filler viscosity and penetration pressure.

The reported quality of drilled hole in filled CFRP/honeycomb structures (Fig. 13b) is comparable to the excellent quality of holes drilled by Lindqvist and Kihlman [25] using helical milling technology. Neither drilling-induced burrs nor delamination was observed. Considering that the operation time of conventional drilling is often eight-times shorter, and the implementation of helical milling is still challenging, it is recommended to apply fillers in the honeycomb core at the hole locations at least and drill holes using conventional drilling cycles.

The experimental results showed that the influence of the factors on the response variables is not significant in the hollow honeycomb core. The reason for this may be that the honeycomb structure resulted in a difficult-to-controlled honeycomb cutting angle (θ —the angle between the cutting speed and the honeycomb wall). For example, if a nominal

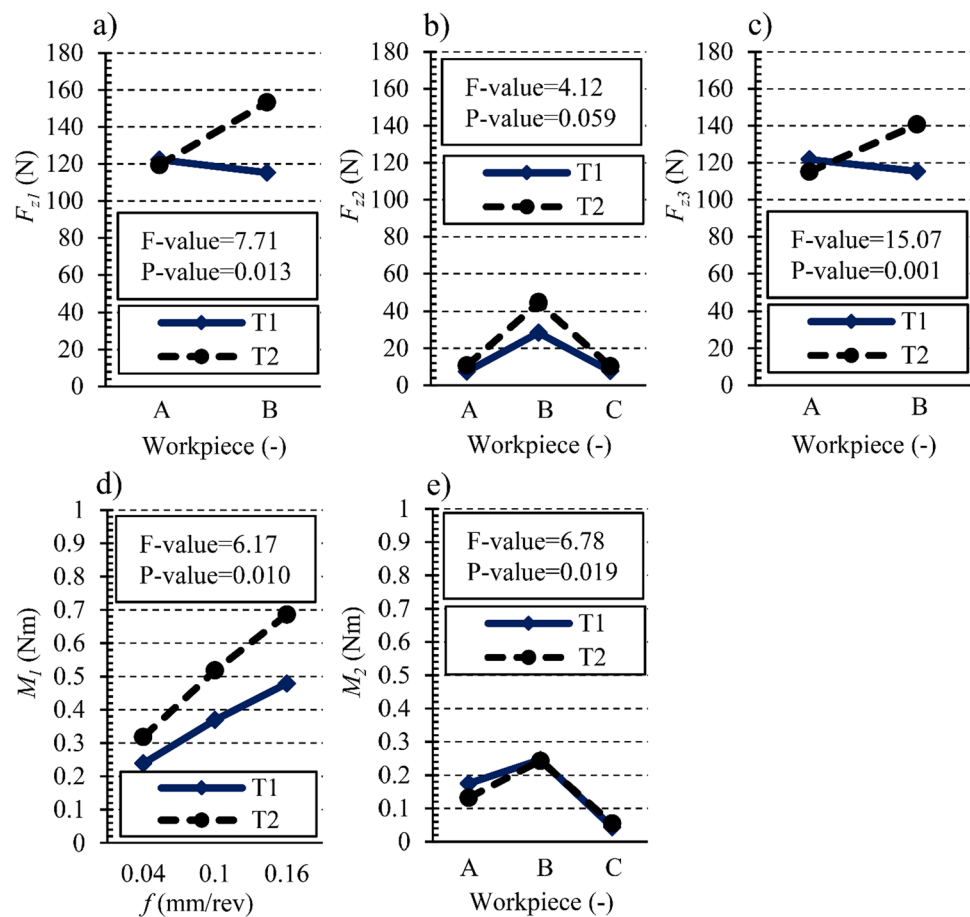
Fig. 9 The main effect plots for the drilling torque (M) in each region



hole position is, as illustrated in Fig. 14a, the honeycomb cutting angle varies between 70° and 110° , and the cutting edge gets in contact with the honeycomb structure $i=9$ times with a quasi-constant distance. However, in the case of the hole position illustrated in Fig. 14b, the range of honeycomb cutting angles is significantly larger: between 14° and 171° ; furthermore, the cutting edge gets in contact with the honeycomb structure $i=14$ times with varying distances. Based on the analogy of the effect of the fibre cutting angle on the chip removal mechanisms in unidirectional CFRPs [39], the closer the cutting angle to 135° , the more bending dominated

the chip removal mechanism expected. As the exact position of the honeycomb structure relative to the hole position is not known because the honeycomb is hidden by the CFRP shells, its control is difficult, and the control of the cutting mechanism of the honeycomb core is therefore challenging, as it was highlighted by Xu et al. also [9]. In addition to the varied honeycomb cutting angles, the honeycomb thickness also differs (t , $2t$) due to the pre-manufacturing processes [40], which makes the design of machining technology of CFRP/honeycomb sandwich structures even more difficult.

Fig. 10 The significant interaction plots for the thrust force (F_z) and drilling torque (M), based on ANOVA at $\alpha=0.05$



Workpiece	T1: twist drill			T2: brad & spur drill		
	$f_1=0.04$ mm/rev	$f_2=0.10$ mm/rev	$f_3=0.16$ mm/rev	$f_1=0.04$ mm/rev	$f_2=0.10$ mm/rev	$f_3=0.16$ mm/rev
A						
B						
C						

Fig. 11 Representative processed images on the drilling-induced burrs and macro-geometrical damages in unfilled (A) and filled (B) CFRP/honeycomb sandwich structures and in single honeycomb (C) structure

As the difficult-to-predict response value (thrust force, burr, etc.) generation in the honeycomb structure was found to result in a difficult-to-optimize machining

process, the monitoring of the position and orientation of the honeycomb core—between the CFRP shells—would significantly improve the design-ability of machining of

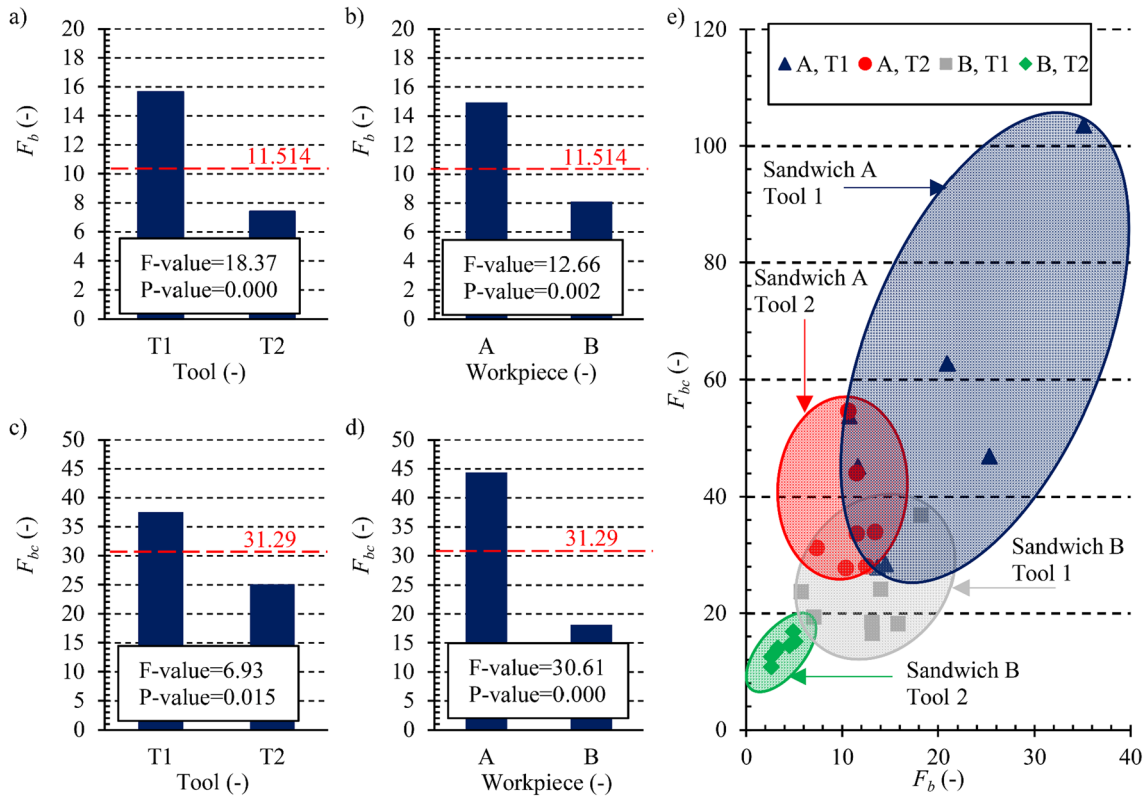
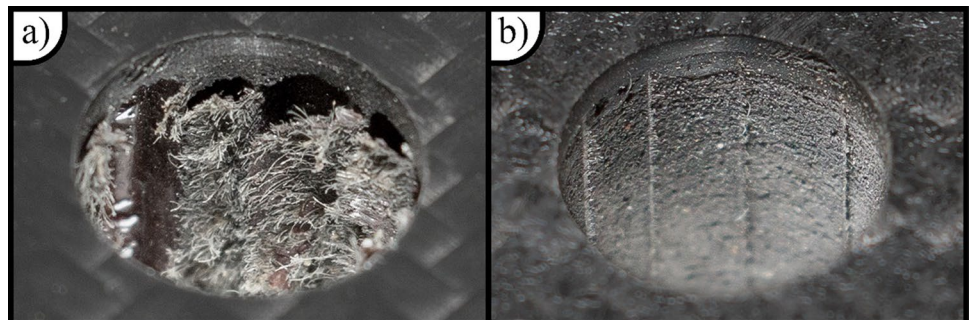


Fig. 12 The main effect plots for the a, b burr factor (F_b) and c, d contour burr factor (F_{bc}), and the d scatterplot of F_b vs F_{bc}

Table 5 ANOVA tables for burr factor and contour burr factor vs feed, tool and workpiece

(a) Burr factor (F_b)						(b) Contour burr factor (F_{bc})					
Source	DF	Adj SS	Adj MS	F value	P value	Source	DF	Adj SS	Adj MS	F value	P value
F_b vs $f = \{f_1; f_2; f_3\}, T = \{T1; T2\}$ and $W = \{A; B\}$						F_{bc} vs $f = \{f_1; f_2; f_3\}, T = \{T1; T2\}$ and $W = \{A; B\}$					
f	2	28.49	14.24	0.55	0.586	f	2	1353	676.47	4.29	0.026
T	1	477.75	477.75	18.37	0.000	T	1	1093	1093.42	6.93	0.015
W	1	329.11	329.11	12.66	0.002	W	1	4826	4825.70	30.61	0.002

Fig. 13 Representative images of drilled hole qualities in a unfilled and b filled CFRP/honeycomb sandwich structures



CFRP/honeycomb sandwich structures. Therefore, considerable attention may be possibly shown in the future

to determine the position and orientation of the hidden honeycomb cores.

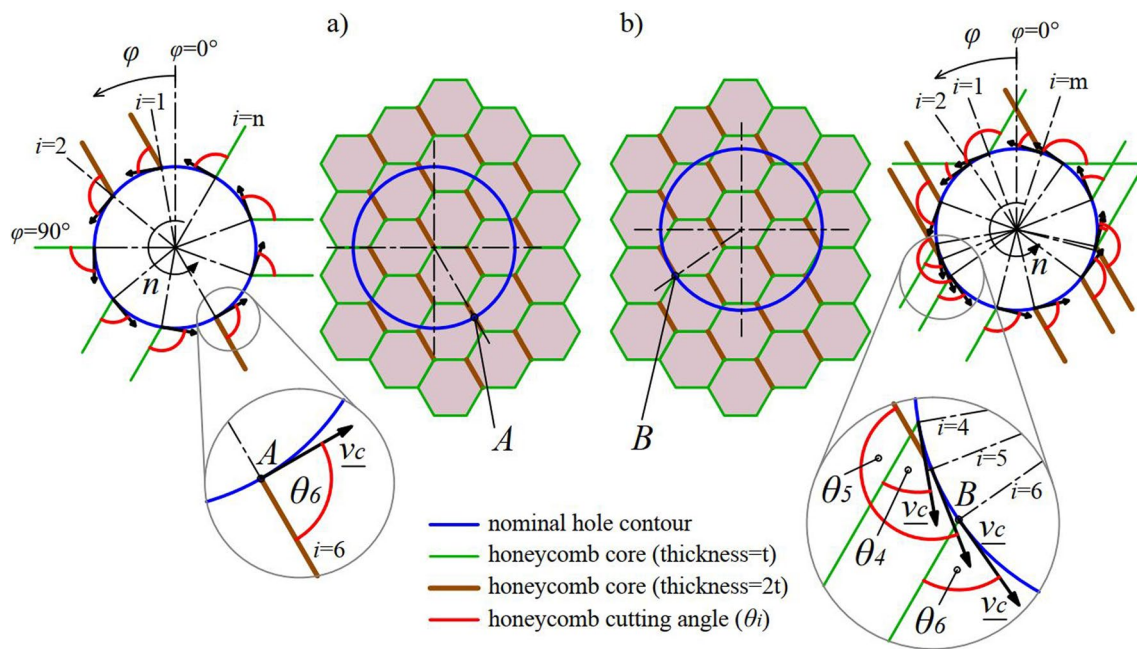


Fig. 14 Schematic illustration of the difficult-to-control honeycomb cutting angle (θ): **a** hole position is advantageous due to the favourable θ , **b** hole position is disadvantageous due to the unfavourable θ

4 Conclusions

In the present study, drilling experiments were conducted in filled and unfilled CFRP/honeycomb sandwich structures at different feeds using different tool geometries. The thrust force, drilling torque, burr factor and contour burr factor parameters were used to characterise and optimise the machining process of these sandwich structures. According to the present study, the following conclusions can be drawn:

- The experimental results show that the twist drill is more advantageous in drilling the CFRP shells, as the achievable hole quality is excellent, and the thrust force and drilling torque are minimal. Nevertheless, the brad and spur drill produced fewer machining-induced burrs in the core of the sandwich structure. Tool selection for drilling CFRP/honeycomb sandwich structures is recommended to include the proper association of these contradictory phenomena.
- It was experimentally proved that applying fillers in the honeycomb only slightly decreased the nominal specific stiffness of the CFRP/honeycomb sandwich structures and slightly increased the thrust force. However, a significant improvement is achievable by their application in the drilling-induced burr formation of the honeycomb core.

- The ANOVA results show that the feed significantly influences the thrust force and drilling torque; however, its influence on the drilling-induced burr characteristics is not considerable.
- It was found that the burr factor and the contour burr factor often do not correlate with each other; therefore, both factors are recommended to be determined for machining process analysis and quality optimisation in CFRP sandwich structures with honeycomb cores.
- Future work is needed to improve the penetrability of the filler into the honeycomb structure and develop novel technologies to determine the position and orientation of the hidden honeycomb structure between the composite shells.

Acknowledgements This research was partly supported by the János Bolyai Research Scholarship of the Hungarian Academy of Sciences No. BO/00508/22/6 and the New National Excellence Program of the Ministry for Innovation and Technology No. ÚNKP-22-5-BME-327. The research reported in this paper is part of Project No. BME-NVA-02, implemented with the support provided by the Ministry of Innovation and Technology of Hungary from the National Research, Development and Innovation Fund, financed under the TKP2021 funding scheme. The author acknowledges the support of Dániel István Poór, Csongor Pereszlai, Alexandra Végh, and especially Gábor Mándi in the experimental work and proofreading.

Author contributions Norbert GEIER's contributions: Conceptualisation, Methodology, Formal analysis, Investigation, Visualisation, Software, Writing—Original Draft.

Funding Open access funding provided by Budapest University of Technology and Economics. Not applicable.

Data availability Not applicable.

Code availability Not applicable.

Declarations

Competing interests Not applicable.

Ethics approval Not applicable.

Consent to participate Not applicable.

Consent for publication Not applicable.

Open Access This article is licensed under a Creative Commons Attribution 4.0 International License, which permits use, sharing, adaptation, distribution and reproduction in any medium or format, as long as you give appropriate credit to the original author(s) and the source, provide a link to the Creative Commons licence, and indicate if changes were made. The images or other third party material in this article are included in the article's Creative Commons licence, unless indicated otherwise in a credit line to the material. If material is not included in the article's Creative Commons licence and your intended use is not permitted by statutory regulation or exceeds the permitted use, you will need to obtain permission directly from the copyright holder. To view a copy of this licence, visit <http://creativecommons.org/licenses/by/4.0/>.

References

- Castanie B, Bouvet C, Ginot M (2020) Review of composite sandwich structure in aeronautic applications. *Compos Part C Open Access* 1:100004. <https://doi.org/10.1016/j.jcomc.2020.100004>
- Alphonse M, Bupesh Raja VK, Gopala Krishna V et al (2021) Mechanical behavior of sandwich structures with varying core material—a review. *Mater Today Proc* 44:3751–3759. <https://doi.org/10.1016/j.matpr.2020.11.722>
- Qi C, Jiang F, Yang S (2021) Advanced honeycomb designs for improving mechanical properties: A review. *Compos Part B Eng* 227:109393. <https://doi.org/10.1016/j.compositesb.2021.109393>
- Le VT, Ha NS, Goo NS (2021) Advanced sandwich structures for thermal protection systems in hypersonic vehicles: a review. *Compos Part B Eng* 226:109301. <https://doi.org/10.1016/j.compositesb.2021.109301>
- Birman V, Kardomateas GA (2018) Review of current trends in research and applications of sandwich structures. *Compos B Eng* 142:221–240. <https://doi.org/10.1016/j.compositesb.2018.01.027>
- Xiang D-H, Wu B-F, Yao Y-L et al (2019) Ultrasonic vibration assisted cutting of Nomex honeycomb core materials. *Int J Precis Eng Manuf* 20:27–36. <https://doi.org/10.1007/s12541-019-00038-8>
- Suresh M, Sanders A, Prajapati P et al (2020) Composite sandwich repair using through-thickness reinforcement with robotic hand micro-drilling. *Compos Struct* 248:112473. <https://doi.org/10.1016/j.compstruct.2020.112473>
- Takács L, Szabó F (2020) Experimental and numerical failure analysis of adhesive joint of glass fiber reinforced polymer composite. *Period Polytech Mech Eng* 64:88–95. <https://doi.org/10.3311/PPme.15106>
- Xu Q, Bao Y, Wang Y-Q, Gao H (2021) Investigation on damage reduction method by varying cutting angles in the cutting process of rectangular Nomex honeycomb core. *J Manuf Process* 68:1803–1813. <https://doi.org/10.1016/j.jmapro.2021.07.006>
- Zarrouk T, Salhi J-E, Atlati S et al (2022) Modeling and numerical simulation of the chip formation process when machining Nomex. *Environ Sci Pollut Res Int* 29:98–105. <https://doi.org/10.1007/s11356-021-13736-6>
- IstvánPoór D, Geier N, Pereszlai C, Xu J (2021) A critical review of the drilling of CFRP composites: Burr formation, characterisation and challenges. *Compos Part B Eng* 223:109155. <https://doi.org/10.1016/j.compositesb.2021.109155>
- Xu J, Li C, Chen M et al (2019) An investigation of drilling high-strength CFRP composites using specialized drills. *Int J Adv Manuf Technol* 103:3425–3442. <https://doi.org/10.1007/s00170-019-03753-8>
- Davim JP (2013) *Machining composites materials*. Wiley
- Davim JP, Rubio JC, Abrao AM (2007) A novel approach based on digital image analysis to evaluate the delamination factor after drilling composite laminates. *Compos Sci Technol* 67:1939–1945. <https://doi.org/10.1016/j.compscitech.2006.10.009>
- Geier N, Xu J, Pereszlai C et al (2021) Drilling of carbon fibre reinforced polymer (CFRP) composites: Difficulties, challenges and expectations. *Procedia Manuf* 54:284–289. <https://doi.org/10.1016/j.promfg.2021.07.045>
- Ahmad S, Zhang J, Feng P et al (2020) Experimental study on rotary ultrasonic machining (RUM) characteristics of Nomex honeycomb composites (NHCs) by circular knife cutting tools. *J Manuf Process* 58:524–535. <https://doi.org/10.1016/j.jmapro.2020.08.023>
- Geier N, Paulo Davim J, Szalay T (2019) Advanced cutting tools and technologies for drilling carbon fibre reinforced polymer (CFRP) composites: a review. *Compos Part A Appl Sci Manuf* 125:105552. <https://doi.org/10.1016/j.compositesa.2019.105552>
- Xiang D, Wu B, Yao Y et al (2019) Ultrasonic longitudinal-torsional vibration-assisted cutting of Nomex® honeycomb-core composites. *Int J Adv Manuf Technol* 100:1521–1530. <https://doi.org/10.1007/s00170-018-2810-3>
- Wu CQ, Gao GL, Li HN, Luo H (2019) Effects of machining conditions on the hole wall delamination in both conventional and ultrasonic-assisted CFRP drilling. *Int J Adv Manuf Technol* 104:2301–2315. <https://doi.org/10.1007/s00170-019-04052-y>
- Ma G, Kang R, Yan C et al (2021) Mechanical model of thrust force and torque in longitudinal-torsional coupled ultrasonic-assisted drilling of CFRP. *Int J Adv Manuf Technol*. <https://doi.org/10.1007/s00170-021-08192-y>
- Kim G, Sterkenburg R, Tsutsui W (2018) Investigating the effects of fluid intrusion on Nomex® honeycomb sandwich structures with carbon fiber facesheets. *Compos Struct* 206:535–549. <https://doi.org/10.1016/j.compstruct.2018.08.054>
- Xie S, Wang H, Yang C et al (2020) Mechanical properties of combined structures of stacked multilayer Nomex® honeycombs. *Thin-Wall Struct* 151:106729. <https://doi.org/10.1016/j.tws.2020.106729>
- Lindqvist R, Eriksson I, Wolf M (2001) Orbital drilling of sandwich constructions for space applications. pp 2001-01-2571
- Kihlman H, Eriksson I, Ennis M (2002) Robotic orbital drilling of structures for aerospace applications. Society of Automotive Engineers, Berlin
- Lindqvist R, Kihlman H (2004) Orbital drilling—implementation and evaluation. pp 2004-01-2814
- Yang B, Wang H, Chen Y et al (2021) Experimental evaluation and modelling of drilling responses in CFRP/honeycomb composite sandwich panels. *Thin-Walled Struct* 169:108279. <https://doi.org/10.1016/j.tws.2021.108279>

27. Khoran M, Ghabezi P, Frahani M, Besharati MK (2015) Investigation of drilling composite sandwich structures. *Int J Adv Manuf Technol* 76:1927–1936. <https://doi.org/10.1007/s00170-014-6427-x>
28. Su F, Zheng L, Sun F et al (2018) Novel drill bit based on the step-control scheme for reducing the CFRP delamination. *J Mater Process Technol* 262:157–167. <https://doi.org/10.1016/j.jmatprotec.2018.06.037>
29. Altintas Y (2012) *Manufacturing automation: metal cutting mechanics, machine tool vibrations, and CNC design*. Cambridge University Press
30. Geier N, Szalay T, Takács M (2018) Analysis of thrust force and characteristics of uncut fibres at non-conventional oriented drilling of unidirectional carbon fibre-reinforced plastic (UD-CFRP) composite laminates. *Int J Adv Manuf Technol* 100:3139–3154. <https://doi.org/10.1007/s00170-018-2895-8>
31. Pereszlai C, Geier N, Poór DI et al (2021) Drilling fibre reinforced polymer composites (CFRP and GFRP): An analysis of the cutting force of the tilted helical milling process. *Compos Struct* 262:113646. <https://doi.org/10.1016/j.compstruct.2021.113646>
32. Sorrentino L, Turchetta S, Bellini C (2018) A new method to reduce delaminations during drilling of FRP laminates by feed rate control. *Compos Struct* 186:154–164. <https://doi.org/10.1016/j.compstruct.2017.12.005>
33. Biró I, Szalay T (2017) Extension of empirical specific cutting force model for the process of fine chip-removing milling. *Int J Adv Manuf Technol* 88:2735–2743. <https://doi.org/10.1007/s00170-016-8957-x>
34. Jáuregui JC, Reséndiz JR, Thenozhi S et al (2018) Frequency and time-frequency analysis of cutting force and vibration signals for tool condition monitoring. *IEEE Access* 6:6400–6410. <https://doi.org/10.1109/ACCESS.2018.2797003>
35. Balázs BZ, Takács M (2020) Experimental investigation and optimisation of the micro milling process of hardened hot-work tool steel. *Int J Adv Manuf Technol* 106:5289–5305. <https://doi.org/10.1007/s00170-020-04991-x>
36. Xu J, Li C, Mi S et al (2018) Study of drilling-induced defects for CFRP composites using new criteria. *Compos Struct* 201:1076–1087. <https://doi.org/10.1016/j.compstruct.2018.06.051>
37. Gaitonde VN, Karnik SR, Rubio JC et al (2008) Analysis of parametric influence on delamination in high-speed drilling of carbon fiber reinforced plastic composites. *J Mater Process Technol* 203:431–438. <https://doi.org/10.1016/j.jmatprotec.2007.10.050>
38. Geier N, Poór DI, Pereszlai C, Tamás-Bényei P (2022) Drilling of recycled carbon fibre-reinforced polymer (rCFRP) composites: analysis of burrs and microstructure. *Int J Adv Manuf Technol*. <https://doi.org/10.1007/s00170-022-08847-4>
39. Li H, Qin X, He G et al (2016) Investigation of chip formation and fracture toughness in orthogonal cutting of UD-CFRP. *Int J Adv Manuf Technol* 82:1079–1088. <https://doi.org/10.1007/s00170-015-7471-x>
40. Karakoç A, Freund J (2012) Experimental studies on mechanical properties of cellular structures using Nomex® honeycomb cores. *Compos Struct* 94:2017–2024. <https://doi.org/10.1016/j.compstruct.2012.01.024>

Publisher's Note Springer Nature remains neutral with regard to jurisdictional claims in published maps and institutional affiliations.